ADVANCES IN ATMOSPHERIC SCIENCES, 2025

• Data Description Article •

Arctic Ocean Dynamical Downscaling Data for Understanding Past and Future Climate Change

Qi SHU[1,2,3,4], Qiang WANG[3], Yan HE[1,2,4], Zhenya SONG[1,2,4], Gui GAO[5], Hailong LIU[6], Shizhu WANG[1,2,4], Rongrong PAN[1,2,4], and Fangli QIAO[*1,2,4]

[1]*First Institute of Oceanography and Key Laboratory of Marine Science and Numerical Modeling, Ministry of Natural Resources, Qingdao, China*

[2]*Laboratory for Regional Oceanography and Numerical Modeling, Qingdao Marine Science and Technology Center, Qingdao, China*

[3]*Alfred Wegener Institute, Helmholtz Centre for Polar and Marine Research (AWI), Bremerhaven, Germany*

[4]*Shandong Key Laboratory of Marine Science and Numerical Modeling, Qingdao, China*

[5]*The Faculty of Geosciences and Environmental Engineering, Southwest Jiaotong University, Chengdu, China*

[6]*Yunnan University, Kunming, China*

(Received 3 July 2024; revised 27 December 2024; accepted 2 January 2025)

ABSTRACT

The Arctic is one of Earth's regions highly susceptible to climate change. However, in situ long-term observations used for climate research are relatively sparse in the Arctic Ocean, and current climate models exhibit notable biases in Arctic Ocean simulations. Here, we present an Arctic Ocean dynamical downscaling dataset, obtained from the global ocean–sea ice model FESOM2 with a regionally refined horizontal resolution of 4.5 km in the Arctic region, which is driven by bias-corrected surface forcings derived from a climate model. The dataset includes 115 years (1900–2014) of historical simulations and two 86-year future projection simulations (2015–2100) for the SSP2-4.5 and SSP5-8.5 scenarios. The historical simulations demonstrate substantially reduced biases in temperature, salinity and sea-ice thickness compared to CMIP6 climate models. Common biases in the representation of the Atlantic Water layer found in climate model simulations are also markedly reduced in the dataset. Serving as a crucial long-term data source for climate change assessments and scientific research for the Arctic Ocean, this dataset provides valuable information for the scientific community.

Key words: Arctic Ocean, climate change, CMIP6, FESOM2, FIO-ESM

Citation: Shu, Q., and Coauthors, 2025: Arctic ocean dynamical downscaling data for understanding past and future climate change. *Adv. Atmos. Sci.*, https://doi.org/10.1007/s00376-025-4259-2.

Database profile	
Database title	Arctic Ocean dynamical downscaling data for understanding past and future climate change
Time range	Historical simulation: 1900–2014 SSP2-4.5 projection: 2015–2100 SSP5-8.5 projection: 2015–2100
Geographical scope	Arctic Ocean
Data format	NetCDF
Data volume	Historical simulation: 427 GB SSP2-4.5 projection: 314 GB SSP5-8.5 projection: 312 GB
Data service system	Historical simulation: https://doi.org/10.57760/sciencedb.16206 SSP2-4.5 projection: https://doi.org/10.57760/sciencedb.16286 SSP5-8.5 projection: https://doi.org/10.57760/sciencedb.16319
Sources of funding	National Key Research and Development Program of China (Grant No. 2023YFF0804600). National Natural Science Foundation of China (Grant Nos. 42276253 and 41821004).

* Corresponding author: Fangli QIAO
Email: qiaofl@fio.org.cn

(Continued.)

Database profile	
Database composition	1. Historical simulation dataset contains 1840 files. Each file contains one-year data for one specific variable. There are 16 ocean/ice variables. 2. SSP2-4.5 projection dataset contains 1376 files. Each file contains one-year data for one specific variable. There are 16 ocean/ice variables. 3. SSP5-8.5 projection dataset contains 1376 files. Each file contains one-year data for one specific variable. There are 16 ocean/ice variables.

1. Background and Summary

Rapid warming in the Arctic has become increasingly evident. Observations and reanalysis datasets show that the Arctic surface is warming at a rate nearly four times faster than the global mean—a phenomenon known as Arctic Amplification (Serreze and Barry, 2011; Chylek et al., 2022; Rantanen et al., 2022). Meanwhile, the Arctic sea ice has declined dramatically, as revealed by satellite observations (Onarheim et al., 2018; Stroeve and Notz, 2018). During the period from 1979 to 2019, the extent of Arctic sea ice in September decreased by 43% (AMAP, 2021). Moreover, significant climate changes have been observed in the Arctic Ocean. Limited in situ observations show a warming trend in the Atlantic Water layer since 1980 (Polyakov et al., 2004). Additionally, there has been a notable accumulation of freshwater in the Arctic Ocean over the last few decades (Rabe et al., 2014; Proshutinsky et al., 2019), with a 6400 km^3 increase in liquid freshwater in the Beaufort Gyre between 2003 and 2018 (Proshutinsky et al., 2019).

The warming and freshening of the Arctic Ocean exert profound impacts on local marine ecosystems and atmosphere–ocean–sea-ice interactions (Coupel et al., 2015; Ardyna and Arrigo, 2020). The accumulation of freshwater in the Arctic Ocean also has the potential to influence the Atlantic Meridional Overturning Circulation when the excess freshwater is released into the sub-polar North Atlantic Ocean (Haine et al., 2023). However, long-term observations in the Arctic Ocean for climate research remain relatively sparse. For example, measurements of ocean volume, heat, and freshwater transports through the four Arctic Ocean gateways (Bering Strait, Fram Strait, Barents Sea Opening, and Davis Strait), which are crucial processes in Arctic Ocean Borealization, have only been conducted with moored instruments since the 1990s. The lateral and/or vertical resolutions of these year-round ocean observations are relatively low, and in some cases, only parts of the straits are covered by moorings (Wang et al., 2023). Long-term observations inside the Arctic Ocean are also severely limited, often covering even shorter periods.

Climate models are widely used for understanding and predicting Arctic Ocean climate changes (Shu et al., 2018, 2021; Haine, 2020; Khosravi et al., 2022). However, state-of-the-art climate models still face essential challenges in the form of large biases and considerable intermodel spread in the Arctic Ocean. For example, the simulated Atlantic Water layer in the Arctic Ocean tends to be too thick and too deep in climate models (Shu et al., 2019; Khosravi et al., 2022). As a result, the simulated warming trend and interannual variability of the Atlantic Water layer appear weaker compared to observations (Shu et al., 2019). Furthermore, the poleward ocean heat transport through the Barents Sea Opening, which is carried by the Barents Sea branch of the Atlantic Water inflow, is underestimated in CMIP5/6 models, both in terms of its mean value and its upward trend. This underestimation contributes to an overly slow decline in sea ice in the Barents Sea (Li et al., 2017; Pan et al., 2023).

The common biases in climate models regarding the Arctic Ocean can often be attributed to the low horizontal resolutions typically used in their ocean component models. Recent ocean–sea-ice model simulations forced by atmospheric reanalysis show that employing higher ocean resolution significantly improves the simulation of the Atlantic Water layer, surface mixed-layer depth, and cold halocline base depth, as well as the Arctic gateway transports (Wang et al., 2024). While ocean reanalysis datasets exhibit relatively small biases, they typically only cover periods starting from the satellite era and lack future projections.

To provide a high quality ocean dataset suitable for Arctic Ocean climate research, we established an Arctic Ocean dynamical downscaling dataset spanning the period from 1900 to 2100. This dataset is based on a high-resolution ocean–sea-ice coupled model and the bias-corrected surface forcings derived from a climate model. It includes 115 years of historical simulations (1900–2014) and two 86-year future projections (2015–2100) aligned with the SSP2-4.5 and SSP5-8.5 scenarios. The two scenarios represent the medium and high ends of future forcing pathways (O'Neill et al., 2016; Riahi et al., 2017), with effective radiative forcings of 4.5 and 8.5 W m^{-2} in 2100, respectively. High-resolution modeling significantly reduces the common biases observed in low-resolution climate models. Therefore, the newly established dataset differs from existing climate model products and reanalysis datasets, providing the research community with a unique and valuable resource for Arctic Ocean climate investigations.

2. Methods

This dataset was established utilizing version 2 of the Finite Volume Sea Ice–Ocean Model (FESOM2) (Danilov et al., 2017; Scholz et al., 2022) and the bias-corrected surface forcings derived from the outputs of FIO-ESM v2.1 (the First Institute of Oceanography–Earth System Model, ver-

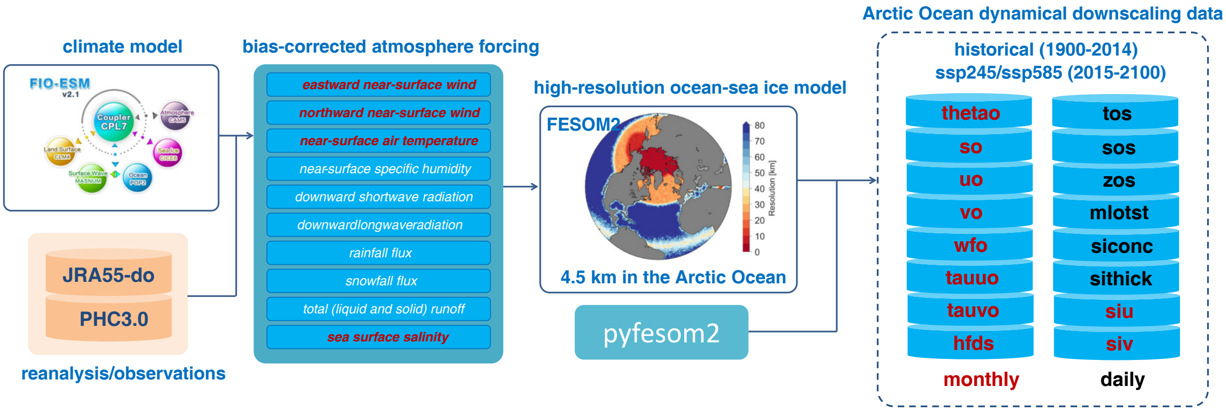

Fig. 1. Framework of the dataset's establishment.

sion 2.1) (Bao et al., 2020; Shu et al., 2024a) within the framework of CMIP6 (Fig. 1). During the dataset's establishment, we implemented bias corrections to the surface forcing fields. The climatological biases of the near-surface wind and near-surface air temperature relative to those from the JRA55-do atmospheric reanalysis (an atmospheric dataset for driving ocean–sea-ice models based on the Japanese 55-year atmospheric reanalysis) (Tsujino et al., 2018) were subtracted.

To facilitate data analysis, we employed the pyfesom2 toolkit, designed for working with FESOM2 ocean model outputs in Python (https://pyfesom2.readthedocs.io/en/latest/index.html) to interpolate FESOM2 outputs from an unstructured mesh onto a regular longitude/latitude grid. In this section, we provide an overview of the ocean–sea-ice model, the surface forcing methodology, and the interpolation employed in this study.

2.1. *FESOM2 and configuration*

FESOM, developed by the Alfred Wegener Institute, stands as the first mature global multi-resolution unstructured-mesh model intended for simulating the global ocean general circulation for climate research (Wang et al., 2014). It can simulate local high-resolution ocean dynamics with variable resolution in a global configuration, thereby reducing computational costs efficiently. FESOM2 is version 2 of FESOM. It includes an ocean general circulation model (Danilov et al., 2017) and a dynamic–thermodynamic sea-ice model, FESIM (Danilov et al., 2015), both operating on the same unstructured triangular meshes. Compared to its predecessor version, FESOM1.4 (Wang et al., 2014, 2018), FESOM2 exhibits higher computational efficiency.

A high horizontal resolution (such as a grid size of 4.5 km) can effectively reduce common Arctic Ocean simulation biases found in low-resolution models (Wang et al., 2018). However, the state-of-the-art climate models in CMIP6 largely employ relatively low resolutions due to the substantial computational costs associated with conducting lengthy climate simulations. In this context, FESOM2 offers a highly suitable platform for conducting long-term, high-resolution dynamical downscaling simulations for the Arctic Ocean. On the one hand, unlike high-resolution fully coupled models or high-resolution global ocean–sea-ice coupled models, whose computational costs are considerable, FESOM2, with computational grid nodes mainly concentrated in the Arctic region, is far less costly. On the other hand, in contrast to regional high-resolution models that require lateral boundary conditions from other simulations, the global multi-resolution unstructured meshes used by FESOM2 eliminate issues associated with lateral boundary conditions. Additionally, FESOM2 demonstrates superior performance in the representation of the Arctic Ocean compared to other global high-resolution models (Wang et al., 2024).

The FESOM mesh we used has ~640 000 surface grid points, which has been used in previous studies with FESOM (Wang et al., 2018, 2019, 2020; Wang and Danilov, 2022). The resolution is 1° in most parts of the global ocean, except in the equatorial belt, where the resolution is 1/3°; north of 50°N, where the resolution is ~25 km; and the Arctic Ocean, where the resolution has been refined to ~4.5 km (Fig. 1). The resolution in the coastal regions has also been increased slightly. The mesh consists of 47 z-levels, featuring a layer thickness of 5 m at the surface, which progressively increases with depth, reaching 250 m towards the bottom. A blend of two high-resolution bottom topography datasets is used (Wang et al., 2018).

In our simulations, vertical mixing is parameterized using the K profile parameterization (Large et al., 1994), with a background diffusivity of 4×10^{-6} m^2 s^{-1} in the Arctic region. Redi (1982) diffusion and the GM parameterization (Gent and McWilliams, 1990) are employed, but deactivated in regions where the horizontal grid spacing is less than half the first baroclinic Rossby radius of deformation. The Redi diffusivity and GM coefficient are scaled with grid spacing in the horizontal direction and vary vertically based on the squared buoyancy frequency. The initial conditions comprise the annual-mean ocean temperature and salinity from version 3.0 of the Polar Science Center Hydrographic Climatology (PHC3.0; Steele et al., 2001). The ocean velocity initially starts from a state of rest. A weak sea surface salinity restoration is used to prevent climate drifts, as suggested in the literature (Griffies et al., 2016).

2.2. *Surface forcing*

The surface forcings used to drive FESOM2 are sourced from the output of FIO-ESM v2.1, which is the latest version of FIO-ESM. FIO-ESM is the first climate model to incorporate the processes of the non-breaking surface wave-induced ocean vertical mixing (Qiao et al., 2004, 2013). With further improvements of air–sea flux exchange processes, FIO-ESM v2.0 participated in CMIP6 (Bao et al., 2020). FIO-ESM v2.0 demonstrates good skill in reproducing the surface air temperature, precipitation, sea surface temperature, Atlantic Meridional Overturning Circulation, El Niño–Southern Oscillation, significant wave height, and other climatological indices of interest in its CMIP6 simulations (Bao et al., 2020; Song et al., 2020; Yang et al., 2023), ranking first for ENSO simulation out of 59 CMIP6 models (Babanin, 2023), and second out of 37 CMIP6 models across 14 CORDEX (Coordinated Regional Downscaling Experiment) domains, including the Arctic (Zhang et al., 2024).

Building upon the successes of its predecessor, FIO-ESM v2.1 has been developed (Shu et al., 2024a) by upgrading the sea-ice component model from the Los Alamos Sea-Ice Model, version 4.0 (CICE4.0) (Hunke and Lipscomb, 2010), to version 6, CICE6.0 (DuVivier, 2018), and improving the physical process of ice–ocean heat exchange from a two-equation boundary condition parameterization to a more realistic three-equation boundary condition parameterization (Shi et al., 2021; Yu et al., 2022). The Arctic sea-ice extent (SIE) simulated by FIO-ESM v2.1 aligns well with satellite observations, and its projected Arctic SIE closely matches observationally constrained projections based on CMIP6 models (Shu et al., 2024a).

The surface forcings derived from FIO-ESM v2.1 include the eastward and northward components of near-surface wind, near-surface air temperature, near-surface specific humidity, surface downward shortwave radiation, surface downward longwave radiation, rainfall flux, snowfall flux, total (liquid and solid) runoff, and sea surface salinity. The spatial resolution for most forcing variables is 1.25° longitude × 0.9° latitude. However, the spatial resolution of total runoff and sea surface salinity is 0.5° longitude × 0.5° latitude and 1.1° longitude × (0.27°–0.54°) latitude, respectively. Most forcing variables have a 3-h temporal interval, except for specific humidity (6-h), total runoff (monthly), and sea surface salinity (monthly).

To reduce FESOM2 simulation errors stemming from biases in the surface forcing derived from FIO-ESM v2.1, we implemented bias corrections to near-surface wind and near-surface air temperature, which are important variables for surface momentum flux and heat flux, respectively, and critical to Arctic ocean and sea-ice simulations. Firstly, we computed the climatological biases of the near-surface wind and near-surface air temperature relative to those from the JRA55-do atmospheric reanalysis (Tsujino et al., 2018) during 1960–2009, at 3-h intervals. JRA55-do was based on the atmospheric reanalysis product JRA-55 by adjusting the original JRA-55 fields using satellite and other atmospheric reanalysis products. JRA55-do is the recommended forcing for driving ocean–sea-ice models in the framework of the Ocean Model Intercomparison Project (OMIP) (Griffies et al., 2016). The climatological biases of near-surface wind speed and near-surface air temperature of FIO-ESM v2.1 relative to those from JRA55-do are shown in Fig. 2. Subsequently, these biases were subtracted from the respective fields for the entire simulation period (1900–2100). Sea surface salinity derived from FIO-ESM v2.1, after bias correction relative to the PHC3.0 monthly climatology, was used for restoring the salinity in FESOM2. The bias correction is applied under the assumption that the biases do not change in the future projection. This may introduce potential uncertainties into future projections.

2.3. *Experimental setup*

Three dynamical downscaling numerical experiments have been conducted, including historical, SSP2-4.5 and SSP5-8.5 simulations (Table 1). The surface forcings for these downscaling simulations are derived from the historical, SSP2-4.5, and SSP5-8.5 experiments of FIO-ESM v2.1,

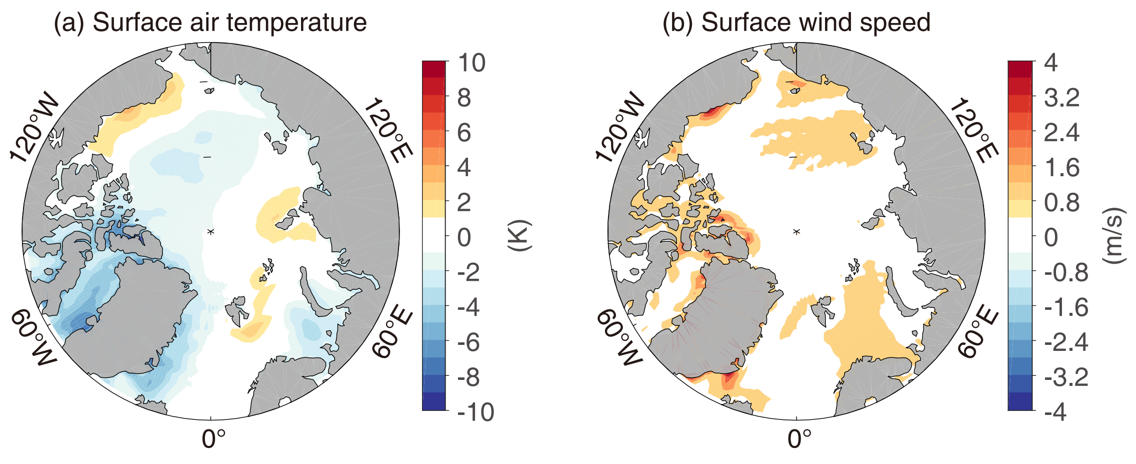

Fig. 2. The climatological biases of the near-surface wind speed and near-surface air temperature of FIO-ESM v2.1 relative to those from the JRA55-do atmospheric reanalysis.

respectively. The historical simulation is initialized from the seawater temperature and salinity of the PHC3.0 climatology, covering the period from 1900 to 2014. The SSP2-4.5 and SSP5-8.5 simulations are future scenario experiments for projecting the future climate under the latest proposed Shared Socioeconomic Pathways. These pathways represent the medium and high ends of future forcing scenarios, corresponding to a 2 K and 4 K warming world, respectively (Tebaldi et al., 2021). Their simulation periods span from 2015 to 2100, and they are initialized on 1 January 2015, using the output from the historical downscaling simulation as the initial conditions.

2.4. *FESOM2 output interpolation*

The output of FESOM is on the model's native unstructured mesh. For the convenience of data usage, the dynamically downscaled results, including both scalar and vector variables, are interpolated onto a regular 0.25° longitude × 0.25° latitude grid using pyfesom2, which is a toolkit for working with FESOM2 ocean model outputs in Python. The interpolation method used is the inverse-distance interpolation. We keep the same vertical layers as the native grid of FESOM2.

3. Data records

This dataset consists of 16 ocean and ice variables (Table 2) from the FESOM2 downscaling experiments, including 115-year historical simulations and two 86-year future scenario (SSP2-4.5 and SSP5-8.5) projections. The dataset covers the area (80°S–90°N, 180°W–180°E) with spatial intervals of 0.25°, so the 2D mesh has 1440 × 680 = 979 200 points in total. The temporal intervals for the dataset vary, with data provided at either monthly mean or daily mean resolutions (Table 2).

The filenames are in the following format, which follows the CMIP6 data filename convention:
<variable_id>_<table_id>_<source_id>_<experiment_id>_<member_id>_<grid_label>_<time_range>.nc,
where <variable_id> is the variable identifier (Table 2), such as thetao, which denotes sea water potential temperature; <table_id> is the table identifier, such as Omon (Oday) and SImon (SIday), which represent the ocean and sea-ice model output with monthly (daily) average values; <source_id> is the model identifier, which is FESOM2 here; <experiment_id> is the experiment identifier, such as historical, ssp245, and ssp585; <member_id> is the variant

Table 1. Dynamical downscaling experiments in this work.

Experiment name	Simulation period	Experiment description	Initial condition
Historical	1900–2014	Historical simulation.	PHC3.0 climatology
SSP2-4.5	2015–2100	Shared Socioeconomic Pathway 245 (SSP2-4.5). The medium part of the range of future forcing pathways, in which the radiative forcing reaches 4.5 W m^{-2} by 2100. It represents a 2 K warming world.	Branched from the historical simulation on 1 January 2015
SSP585	2015–2100	Shared Socioeconomic Pathway 585 (SSP5-8.5). The high end of the range of future forcing pathways, in which the radiative forcing reaches 8.5 W m^{-2} by 2100. It represents a 4 K warming world.	

Table 2. List of all variables in the dataset.

No.	<variable_id>	Description	Units	Dimensions	Frequency
1	thetao	seawater potential temperature	°C	[lon, lat, dep, time]*	monthly mean
2	so	seawater salinity	psu	[lon, lat, dep, time]	monthly mean
3	uo	seawater eastward velocity	m s^{-1}	[lon, lat, dep, time]	monthly mean
4	vo	seawater northward velocity	m s^{-1}	[lon, lat, dep, time]	monthly mean
5	wfo	water flux into seawater	kg m^{-2} s^{-1}	[lon, lat, time]	monthly mean
6	tauuo	seawater surface downward eastward stress	N m^{-2}	[lon, lat, time]	monthly mean
7	tauvo	seawater surface downward northward stress	N m^{-2}	[lon, lat, time]	monthly mean
8	hfds	downward heat flux at seawater surface	W m^{-2}	[lon, lat, time]	monthly mean
9	tos	sea surface temperature	°C	[lon, lat, time]	daily mean
10	sos	sea surface salinity	psu	[lon, lat, time]	daily mean
11	zos	sea surface height	m	[lon, lat, time]	daily mean
12	mlotst	ocean mixed-layer thickness	m	[lon, lat, time]	daily mean
13	siconc	sea-ice concentration	%	[lon, lat, time]	daily mean
14	sithick	sea-ice thickness	m	[lon, lat, time]	daily mean
15	siu	sea-ice eastward velocity	m s^{-1}	[lon, lat, time]	monthly mean
16	siv	sea-ice northward velocity	m s^{-1}	[lon, lat, time]	monthly mean

* lon, lat, and dep represent longitude, latitude and depth, respectively.

label, which is r1i1p1f1 here; <grid_label> is the grid identifier, which is gr here, meaning the output is not reported on the native grid but is regridded to a primary grid; and <time_range> specifies the temporal range covered by the data contained within the file, such as 199501–199512, which means the temporal range is from January 1995 to December 1995.

In this dataset, each file contains one-year data for one specific variable, so there are 16 × 115 = 1840 files for the historical experiment, and 16 × 86 = 1376 files for each future scenario projection experiment.

All data files are archived in ScienceDB (Shu et al., 2024b, 2024c, 2024d) and are provided in NetCDF format. NetCDF files are platform-independent and self-describing, which contain metadata, data structure, dimensions, variables, and attributes. In this dataset, the attribute of “Fill Value” denotes land points.

4. Technical validation

To validate the climatological state of the downscaling simulations, we compared the dynamically downscaled climatological temperature and salinity profiles, Atlantic Water core depth (AWCD), cold halocline base depth, liquid freshwater content, sea surface height, and sea-ice thickness with the results based on the PHC3.0 climatology, satellite observations, and CMIP6 climate models. Including CMIP6 in the comparison is merely intended to demonstrate the benefits of using our dataset for understanding climate change in the Arctic Ocean. We would like to emphasize that our dataset is obtained from downscaling a forced ocean–ice model, while CMIP6 models are coupled climate models. Since long-term observations in the Arctic Ocean are quite sparse, to validate the long-term trend simulated in the downscaling simulations, we only compared the simulated seawater temperature anomalies with a long-term in situ observation in the Barents Sea, and compared the simulated Arctic SIE with satellite-derived SIE.

4.1. *Temperature profile*

The potential temperature profile in the Arctic Basin in the FESOM2 downscaling simulations fits the PHC3.0 climatology well, and its error is much smaller than in the CMIP6 climate models (Fig. 3 and Fig. 4). Previous studies show

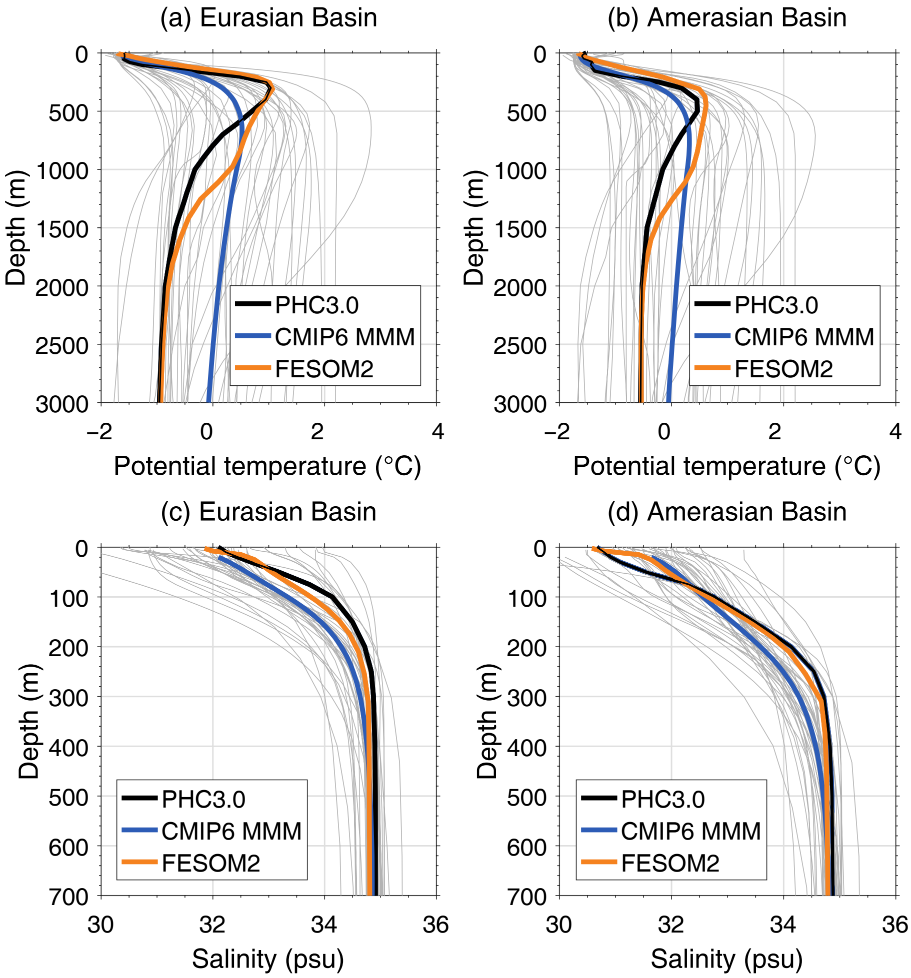

Fig. 3. (a, b) Potential temperature and (c, d) salinity profiles averaged from 1961 to 2000 in the (a, c) Eurasian Basin and (b, d) Amerasian Basin. The thin gray lines are the results from 40 CMIP6 models. The black, blue, and orange thick lines are the results from the PHC3.0 climatology, CMIP6 MMM, and FESOM2 downscaling simulations, respectively.

that climate models have large errors and intermodel spread in the simulated temperature and salinity in the Arctic Ocean (Shu et al., 2019; Khosravi et al., 2022; Heuzé et al., 2023). Figures 3a and b demonstrate that the most recent CMIP6 climate models exhibit large temperature errors in both the Eurasian Basin and the Amerasian Basin. The downscaling simulations exhibit relatively small errors. The root-mean-square error (RMSE) of temperature profiles for most CMIP6 climate models exceeds 0.5°C in the Arctic Basin, with the CMIP6 multimodel mean (MMM) RMSE at 0.64°C (Fig. 4a). In comparison, the RMSE for the downscaling simulations is 0.26°C, which is less than half of the CMIP6 MMM. Additionally, it is lower than the RMSE (0.40°C) of the MMM results from the ocean–sea-ice models in OMIP2 (Griffies et al., 2016).

4.2. *Salinity profile*

Similar to the potential temperature profiles, the salinity profiles in the Arctic Basin are also much better simulated in the downscaling simulations than in the CMIP6 climate models (Fig. 3 and Fig. 4). The CMIP6 climate models exhibit large salinity errors and intermodel spread in the upper 400 m for both the Eurasian and Amerasian basins (Figs. 3c and d). Most climate models are too fresh in the halocline (Figs. 3c and d), causing the halocline to be too deep—a bias that could lead to an underestimation of the possibility of future abrupt Arctic climate change (Jansen et al., 2020). The downscaling simulations show relatively small errors (Fig. 3 and Fig. 4). The RMSE of the salinity profiles in the Arctic Basin in the downscaling simulations is 0.14 psu, which is about half the RMSE of the CMIP6 (0.29 psu) and OMIP2 (Griffies et al., 2016) (0.28 psu) MMM salinity.

4.3. *Atlantic Water layer*

The Atlantic-origin warm water plays an important role in Arctic Ocean climate change. The observed phenomenon of Arctic Atlantification is mainly caused by the increase of the poleward ocean heat transport in the Atlantic Water (Årthun et al., 2012; Polyakov et al., 2020; Shu et al., 2021). Climate models show that future rapid warming of the Atlantic Water layer in the Arctic Ocean may cause the Arctic Ocean to warm faster than the global ocean on average—a phenomenon called Arctic Ocean amplification (Shu et al., 2022). However, the Atlantic Water layer simulated in climate models has large biases (Fig. 3 and Fig. 5). Figures 3a and b indicate that the CMIP6 MMM underestimates the Atlantic Water core temperature (AWCT), which is the maximum temperature of the Atlantic Water layer, and overestimates the AWCD, which is the depth of the AWCT. The potential temperature along the section of 70°E–145°W in Fig. 5 shows there are large discrepancies between the CMIP6 climate models and the PHC3.0 climatology. Some climate models do not have a warm (warmer than 0°C) Atlantic Water layer, and many climate models simulate an overly deep and thick Atlantic Water layer. The Atlantic Water layer is much better reproduced in the downscaling simulations than in the CMIP6 climate models (Fig. 3, Fig. 5, and Fig. 6). The AWCT in the downscaling simulations fits the PHC3.0 climatology well in both the Eurasian and Amerasian basins (Figs. 3a and b). The average AWCD is 310 and 460 m in the Eurasian and Amerasian basins, respectively, based on the PHC3.0 climatology. In the downscaling simulation, the AWCD is 302 and 445 m in the Eurasian and Amerasian basins, respectively—very close to the observations (Fig. 6). On the contrary, the CMIP6

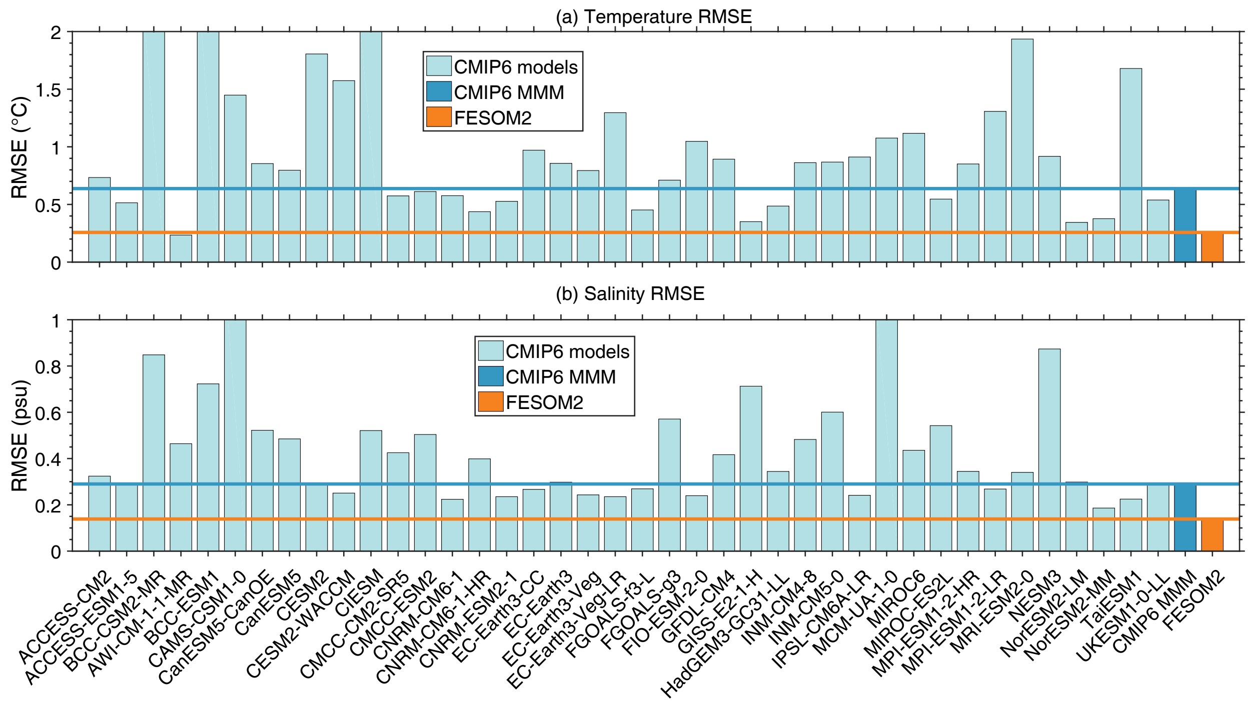

Fig. 4. RMSE of (a) potential temperature and (b) salinity profiles in the Arctic Basin. The light blue, blue, and orange bars represent the results of CMIP6 individual models, the CMIP6 MMM, and FESOM2 downscaling simulations, respectively.

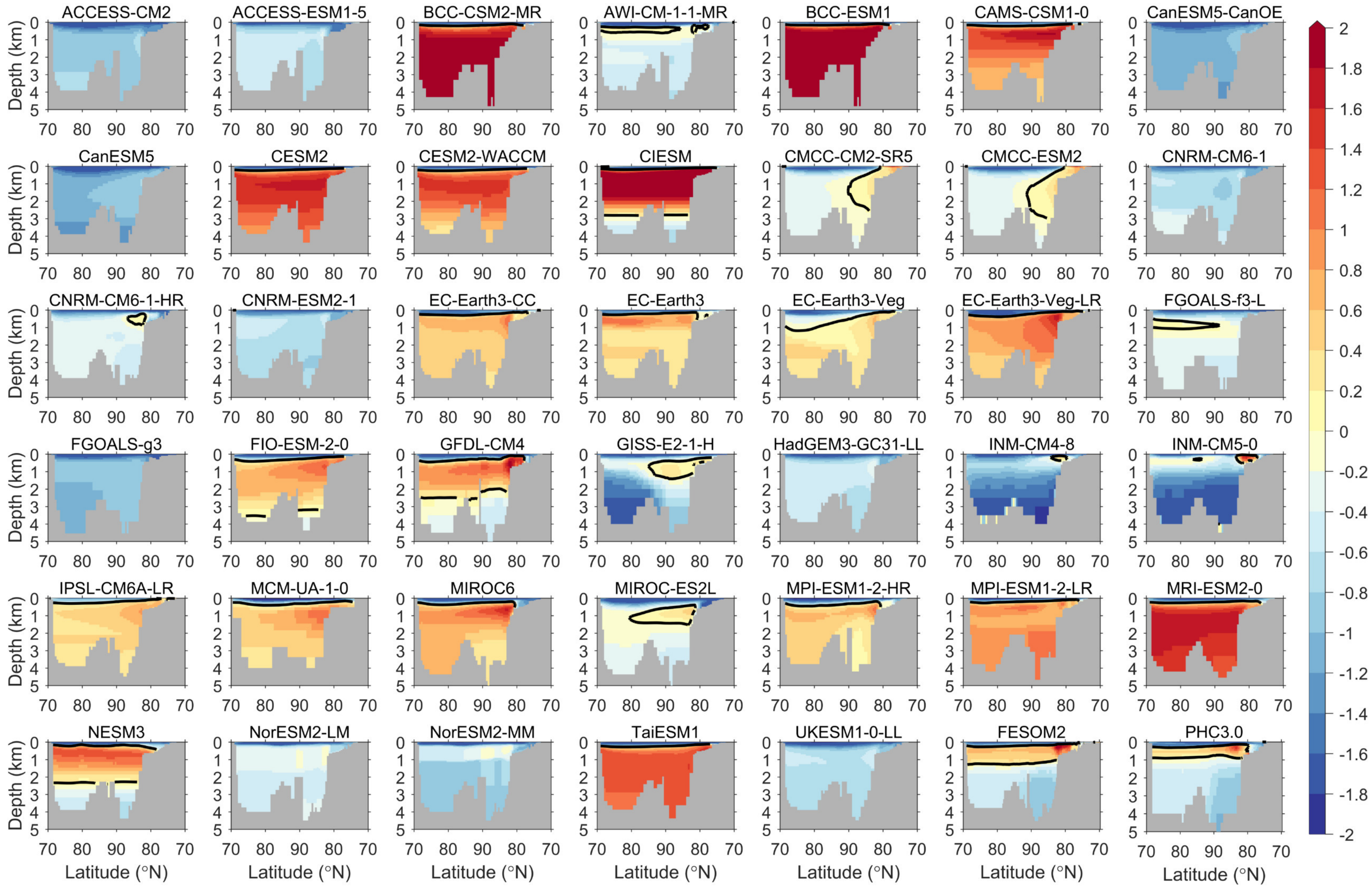

Fig. 5. Vertical section of potential temperature (units: °C) along the 70°E–145°W transect from 40 CMIP6 climate models, FESOM2 downscaling simulations, and the PHC3.0 climatology. The black lines depict the 0°C isotherm, which can be considered as the boundary of the Atlantic Water layer.

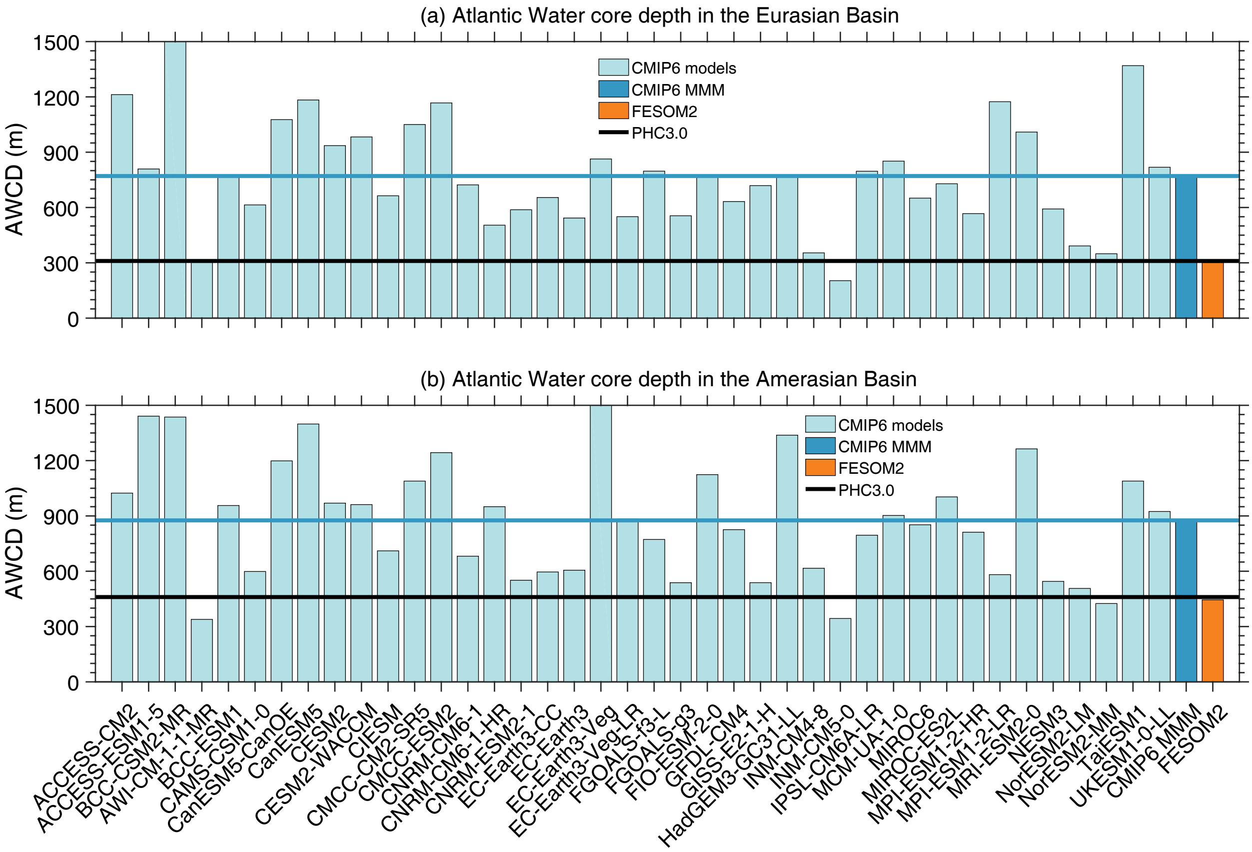

Fig. 6. The AWCD (units: m) in the (a) Eurasian Basin and (b) Amerasian Basin. The light blue, blue, and orange bars represent the results of CMIP6 individual models, the CMIP6 MMM, and FESOM2 downscaling simulations, respectively. The black lines depict the AWCD from the PHC3.0 climatology.

MMM AWCD is 771 and 876 m in the Eurasian and Amerasian basins, respectively—nearly double the observations.

4.4. *Cold halocline base depth*

The cold halocline layer in the Arctic Ocean is an important insulator between the underlying warm Atlantic Water layer and the cold surface mixed layer and sea ice above. The cold halocline base depth is defined as the depth where the ratio of the density gradient due to temperature to the density gradient due to salinity equals 0.05 (Bourgain and Gascard, 2011), so it characterizes the transition from halocline to thermocline. It is shallow in the Eurasian Basin and deep in the Amerasian Basin according to the PHC3.0 climatology (Fig. 7a). There is a large discrepancy between the observations and CMIP6 simulations (Figs. 7a and c). Climate models overestimate the cold halocline base depth significantly in both the Eurasian Basin and Amerasian Basin. In the Amerasian Basin, the observed cold halocline base depth is between 120 and 210 m. However, the cold halocline base depth is deeper than 300 m based on the CMIP6 MMM. Figure 7b indicates that the model result in the downscaling simulations fits the PHC3.0 climatology well, with much smaller biases than climate models.

4.5. *Liquid freshwater content*

The liquid freshwater content (FWC) in the Arctic Ocean has strong implications for the local physical and biogeochemical environment as well as the large-scale ocean circulation in the North Atlantic (Coupel et al., 2015; Ardyna and Arrigo, 2020; Haine et al., 2023). We used the liquid freshwater column (units: m) to validate the downscaling simulations. It is calculated as follows:

$$\mathrm{FWC} = \int_{-H_{\mathrm{ref}}}^{0} \left(1 - S\,(z)\,/S_{\mathrm{ref}}\right) \mathrm{d}z\,,$$

where $S\,(z)$ is the salinity at depth z, $S_{\mathrm{ref}} = 34.8$psu is the reference salinity, and H_{ref} is the depth where the seawater salinity is equal to the reference salinity. The liquid freshwater column is widely used to evaluate model simulations (Zanowski et al., 2021; Wang et al., 2022). The PHC3.0 climatology shows that the liquid freshwater column in the Arctic Ocean is highest in the Beaufort Gyre, and relatively low in the Eurasian Basin (Fig. 7d). Downscaling simulations can reproduce the spatial pattern well and outperform the CMIP6 MMM results (Figs. 7d–f). The total liquid FWC in the Arctic Ocean is 52.4×10^3 km^3 in the downscaling simulations, which is close to the value of 55.8×10^3 km^3 based on the PHC3.0 climatology. However, it is 80.5×10^3 km^3 based on the CMIP6 MMM results.

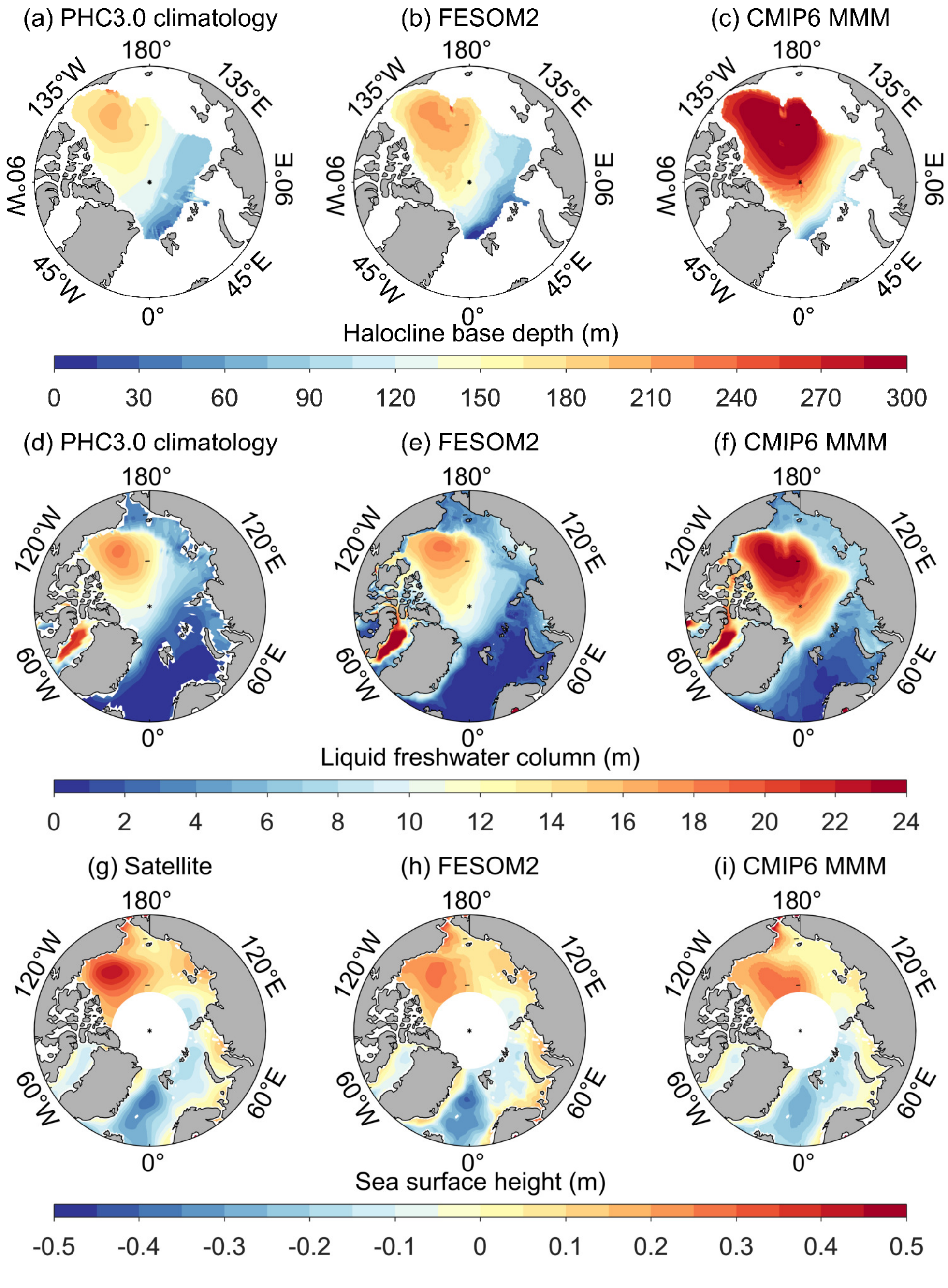

Fig. 7. The (a–c) halocline base depth, (d–f) liquid freshwater column, and (g–i) sea surface height in the Arctic Ocean from observations, FESOM2 downscaling simulations, and the CMIP6 MMM. The halocline base depth and liquid freshwater column are the averaged results during 1961 to 2000. The sea surface height is the averaged result during 2003 to 2014. The mean sea surface height over the latitudinal range between 65°N and 80°N has been removed.

4.6. *Sea surface height*

To evaluate the upper-ocean circulation in the Arctic Ocean, we compared the downscaling simulation's sea surface height with the CMIP6 MMM and the observational estimates from altimetry measurements for the period 2003–14 (Armitage et al., 2016). Figure 7g shows that there is a high in the Beaufort Sea associated with the anticyclonic Beaufort Gyre, a low in the Greenland Sea associated with the cyclonic Greenland Sea gyre, and a large-scale gradient associated with the Transpolar Drift stream (Armitage et al., 2016). Figure 7h indicates that, despite a relatively weak Beaufort Gyre, the downscaling simulations can largely reproduce the spatial pattern observed by satellite. Downscaling simulations are better than the CMIP6 MMM (Fig. 7i). The sea surface height in the Kara Sea, Laptev Sea, and East

Siberian Sea is underestimated by the CMIP6 MMM, and the center of the Beaufort Gyre in the CMIP6 MMM is biased poleward.

4.7. *Time series of ocean temperature in the Barents Sea*

To evaluate the simulated long-term trend, we compared the simulated ocean temperature anomalies with observations and CMIP6 climate model simulations along the Kola Section in the Barents Sea. Figure 8 shows that the observed ocean warming trend along this section is simulated well by FESOM2. The linear trend of the upper 200-m seawater temperature during 1951–2021 along the Kola Section is (0.16 ± 0.05)°C (10 yr)$^{-1}$ and (0.13 ± 0.04)°C (10 yr)$^{-1}$ based on observations and downscaling simulations, respectively, while it is (0.26±0.03)°C (10 yr)$^{-1}$ based on the CMIP6 MMM. Since the surface forcings of the downscaling simulations are derived from a climate model, the phase of the simulated interannual variability is different from in the observations, as expected. However, the amplitudes of the simulated interannual variability are in agreement with the observations.

4.8. *Time series of Arctic SIE*

Satellite observations show that the Arctic exhibits maximum and minimum SIE in March and September, respectively. We compared the time series of the March and September Arctic SIE in the downscaling simulations with the satellite observations and the CMIP6 results (Fig. 9). Figure 9 indicates that the CMIP6 individual models have remarkable intermodel spread, and the downscaling simulations can ably reproduce the satellite-observed mean and the long-term trend of SIE in both March and September, while the downscaling simulations overestimate the September SIE during 2007–13. In March, the SIE climatology during 1979–2020 based on satellite observations is 15.3 × 10^{6} km^{2}, while it is 15.6 × 10^{6} km^{2} based on the downscaling simulations and 15.8 × 10^{6} km^{2} based on the CMIP6 MMM. In September, the SIE mean and long-term trend during 1979–2020 based on satellite observations are 6.0×10^{6} km^{2} and (−0.83 ± 0.13) × 10^{6} km^{2} (10 yr)$^{-1}$, respectively, while they are 6.3×10^{6} km^{2} and (−0.82 ± 0.16) × 10^{6} km^{2} (10 yr)$^{-1}$ based on downscaling simulations, and 6.2 × 10^{6} km^{2} and (−0.58 ± 0.04) × 10^{6} km^{2} (10 yr)$^{-1}$ based on the CMIP6 MMM, respectively.

4.9. *Arctic sea-ice thickness*

To evaluate the simulations of Arctic sea-ice thickness, Fig. 10 shows the cold season (October–April) Arctic sea-ice thickness based on satellite observations (combination of CryoSat-2 and SMOS datasets; Ricker et al., 2017), FESOM2 downscaling simulations, and the CMIP6 MMM during the period 2011–22. Satellite-based observations reveal that thick sea ice is concentrated along the northern coast of the Canadian Arctic Archipelago and Greenland, and the sea-ice thickness in the Barents Sea, Kara Sea, Laptev Sea, and Baffin Bay is relatively thin. Both the FESOM2 downscaling simulations and the CMIP6 MMM can reproduce the spatial pattern of satellite-based observations. However, the FESOM2 downscaling simulations tend to overestimate the sea-ice thickness, while the CMIP6 MMM underestimates it in thick-ice regions and overestimates it in thin-ice regions. This suggests that both models have relatively large biases in simulating sea-ice thickness.

Usage notes This dataset is not a reanalysis dataset since there is no ocean data assimilation used. Data covering only the Arctic Ocean and data on the model's native unstructured mesh are also

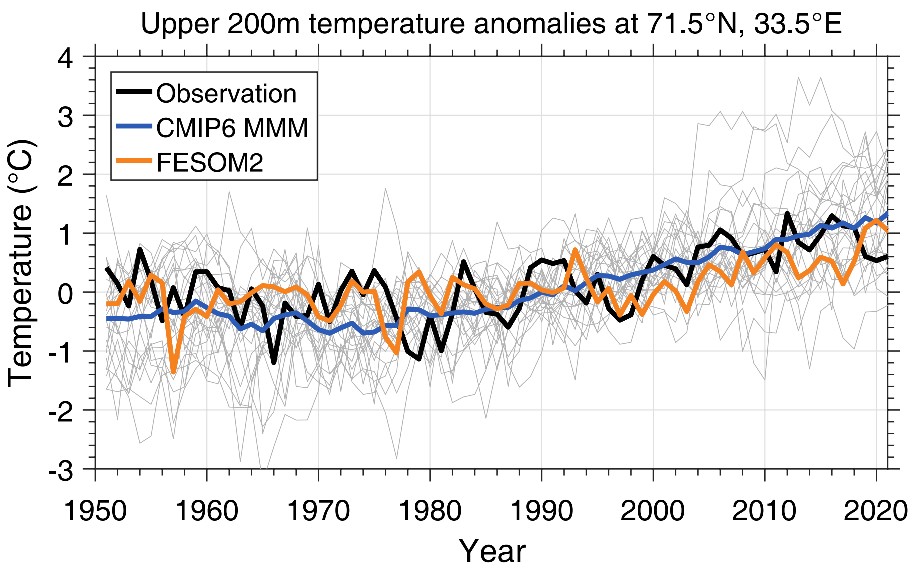

Fig. 8. Upper 200-m seawater temperature anomalies (units: °C) along the Kola Section (centered at 71.5°N, 33.5°E) in the Barents Sea. The thin gray lines are the results from CMIP6 models. The black, blue, and orange thick lines are the results from observations, the CMIP6 MMM, and FESOM2 downscaling simulations, respectively.

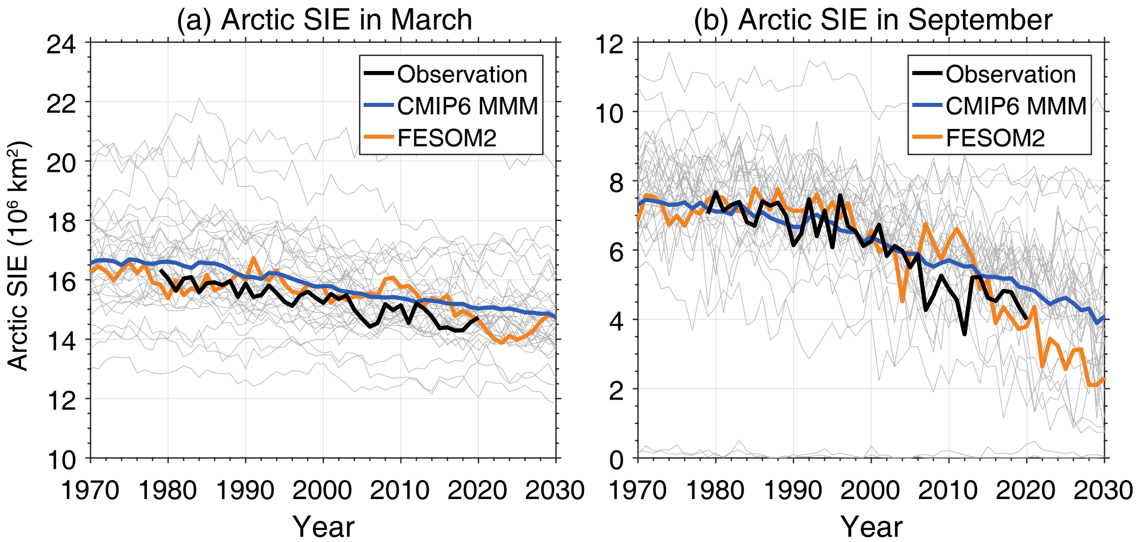

Fig. 9. Arctic SIE in (a) March and (b) September. The gray thin lines represent the results from individual CMIP6 models. The black, blue, and orange thick lines are the results from the satellite observations, CMIP6 MMM, and FESOM2 downscaling simulations, respectively.

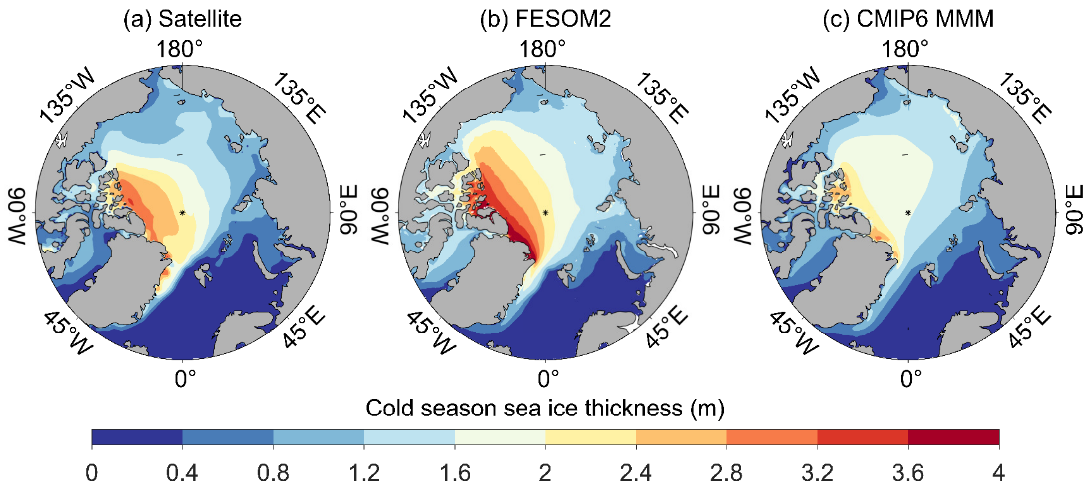

Fig. 10. Cold season (October–April) Arctic sea-ice thickness from satellite observations, FESOM2 downscaling simulations, and the CMIP6 MMM during the period 2011–22.

available from the corresponding author upon request. The surface forcings to drive FESOM2 are also provided in NetCDF format and archived in ScienceDB (Shu, 2024a, 2024b, 2024c). Their filename format also follows the CMIP6 data filename convention.

Acknowledgements. This work was supported by the National Key Research and Development Program of China (Grant No. 2023YFF0804600), the National Natural Science Foundation of China (Grant Nos. 42276253 and 41821004), the Shandong Provincial Natural Science Foundation (Grant No. ZR2022JQ17), and the Taishan Scholar Foundation of Shandong Province (Grant No. tsqn202211264). The PHC3.0 climatology, Kola section observations, satellite-observed SIE and sea-ice thickness are from http://psc.apl.washington.edu/nonwp_projects/PHC/Climatology.html, https://ocean.ices.dk/core/iroc, https://nsidc.org/data/g02135, and https://data.seaiceportal.de/relaunch/thickness?lang=en, respectively. We would like to thank the above data providers.

REFERENCES

AMAP, 2021: Arctic Climate Change Update 2021: Key Trends and Impacts. Summary for Policy-makers. Arctic Monitoring and Assessment Programme.

Ardyna, M., and K. R. Arrigo, 2020: Phytoplankton dynamics in a changing Arctic Ocean. *Nature Climate Change*, **10**, 892–903, https://doi.org/10.1038/s41558-020-0905-y.

Armitage, T. W. K., S. Bacon, A. L. Ridout, S. F. Thomas, Y. Aksenov, and D. J. Wingham, 2016: Arctic sea surface height variability and change from satellite radar altimetry and GRACE, 2003–2014. *J. Geophys. Res.: Oceans*, **121**, 4303–4322, https://doi.org/10.1002/2015JC011579.

Årthun, M., T. Eldevik, L. H. Smedsrud, Ø. Skagseth, and R. B. Ingvaldsen, 2012: Quantifying the influence of Atlantic heat on Barents Sea ice variability and retreat. *J. Climate*, **25**, 4736–4743, https://doi.org/10.1175/JCLI-D-11-00466.1.

Babanin, A. V., 2023: Ocean waves in large-scale air-sea weather and climate systems. *J. Geophys. Res.: Oceans*, **128**, e2023JC019633, https://doi.org/10.1029/2023JC019633.

Bao, Y., Z. Y. Song, and F. L. Qiao, 2020: FIO-ESM version 2.0: Model description and evaluation. *J. Geophys. Res.: Oceans*, **125**, e2019JC016036, https://doi.org/10.1029/2019JC016036.

Bourgain, P., and J. C. Gascard, 2011: The Arctic Ocean halocline and its interannual variability from 1997 to 2008. *Deep Sea Research Part I: Oceanographic Research Papers*, **58**, 745–756, https://doi.org/10.1016/j.dsr.2011.05.001.

Chylek, P., C. Folland, J. D. Klett, M. Y. Wang, N. Hengartner, G. Lesins, and M. K. Dubey, 2022: Annual mean arctic amplification 1970–2020: Observed and simulated by CMIP6 climate models. *Geophys. Res. Lett.*, **49**, e2022GL099371, https://doi.org/10.1029/2022GL099371.

Coupel, P., D. Ruiz-Pino, M. A. Sicre, J. F. Chen, S. H. Lee, N. Schiffrine, H. L. Li, and J. C. Gascard, 2015: The impact of freshening on phytoplankton production in the Pacific Arctic Ocean. *Progress in Oceanography*, **131**, 113–125, https://doi.org/10.1016/j.pocean.2014.12.003.

Danilov, S., D. Sidorenko, Q. Wang, and T. Jung, 2017: The Finite-volumE Sea ice–Ocean Model (FESOM2). *Geoscientific Model Development*, **10**, 765–789, https://doi.org/10.5194/gmd-10-765-2017.

Danilov, S., Q. Wang, R. Timmermann, N. Iakovlev, D. Sidorenko, M. Kimmritz, T. Jung, and J. Schröter, 2015: Finite-Element Sea Ice Model (FESIM), version 2. *Geoscientific Model Development*, **8**, 1747–1761, https://doi.org/10.5194/gmd-8-1747-2015.

DuVivier, A., 2018: CICE-Consortium Documentation. Available from https://buildmedia.readthedocs.org/media/pdf/cicea/latest/cicea.pdf.

Gent, P. R., and J. C. McWilliams, 1990: Isopycnal mixing in ocean circulation models. *J. Phys. Oceanogr.*, **20**, 150–155, https://doi.org/10.1175/1520-0485(1990)020<0150:IMIOCM>2.0.CO;2.

Griffies, S. M., and Coauthors, 2016: OMIP contribution to CMIP6: Experimental and diagnostic protocol for the physical component of the Ocean Model Intercomparison Project. *Geoscientific Model Development*, **9**, 3231–3296, https://doi.org/10.5194/gmd-9-3231-2016.

Haine, T. W. N., 2020: Arctic Ocean freshening linked to anthropogenic climate change: All hands on deck. *Geophys. Res. Lett.*, **47**, e2020GL090678, https://doi.org/10.1029/2020GL090678.

Haine, T. W. N., A. H. Siddiqui, and W. R. Jiang, 2023: Arctic freshwater impact on the Atlantic Meridional Overturning Circulation: Status and prospects. *Philosophical Transactions of the Royal Society A: Mathematical, Physical and Engineering Sciences*, **381**, 20220185, https://doi.org/10.1098/rsta.2022.0185.

Heuzé, C., H. Zanowski, S. Karam, and M. Muilwijk, 2023: The deep Arctic Ocean and Fram Strait in CMIP6 models. *J. Climate*, **36**, 2551–2584, https://doi.org/10.1175/JCLI-D-22-0194.1.

Hunke, E. C., and W. H. Lipscomb, 2010: CICE: The Los Alamos sea ice model documentation and software user's manual version 4.0 LA-CC-06-012. Tech. Rep. LA-CC-06-012.

Jansen, E., and Coauthors, 2020: Past perspectives on the present era of abrupt Arctic climate change. *Nature Climate Change*, **10**, 714–721, https://doi.org/10.1038/s41558-020-0860-7.

Khosravi, N., Q. Wang, N. Koldunov, C. Hinrichs, T. Semmler, S. Danilov, and T. Jung, 2022: The Arctic Ocean in CMIP6 Models: Biases and projected changes in temperature and salinity. *Earth's Future*, **10**, e2021EF002282, https://doi.org/10.1029/2021EF002282.

Large, W. G., J. C. McWilliams, and S. C. Doney, 1994: Oceanic vertical mixing: A review and a model with a nonlocal boundary layer parameterization. *Rev. Geophys.*, **32**, 363–403, https://doi.org/10.1029/94RG01872.

Li, D. W., R. Zhang, and T. R. Knutson, 2017: On the discrepancy between observed and CMIP5 multi-model simulated Barents Sea winter sea ice decline. *Nature Communications*, **8**, 14991, https://doi.org/10.1038/ncomms14991.

Onarheim, I. H., T. Eldevik, L. H. Smedsrud, and J. C. Stroeve, 2018: Seasonal and regional manifestation of Arctic Sea ice loss. *J. Climate*, **31**, 4917–4932, https://doi.org/10.1175/JCLI-D-17-0427.1.

O'Neill, B. C., and Coauthors, 2016: The scenario model intercomparison project (ScenarioMIP) for CMIP6. *Geoscientific Model Development*, **9**, 3461–3482, https://doi.org/10.5194/gmd-9-3461-2016.

Pan, R. R., Q. Shu, Z. Y. Song, S. Z. Wang, Y. He, and F. L. Qiao, 2023: Simulations and projections of Winter Sea ice in the Barents Sea by CMIP6 climate models. *Adv. Atmos. Sci.*, **40**, 2318–2330, https://doi.org/10.1007/s00376-023-2235-2.

Polyakov, I. V., and Coauthors, 2004: Variability of the intermediate Atlantic water of the Arctic Ocean over the last 100 years. *J. Climate*, **17**, 4485–4497, https://doi.org/10.1175/JCLI-3224.1.

Polyakov, I. V., and Coauthors, 2020: Borealization of the Arctic Ocean in response to anomalous advection from sub-Arctic seas. *Frontiers in Marine Science*, **7**, 491, https://doi.org/10.3389/fmars.2020.00491.

Proshutinsky, A., and Coauthors, 2019: Analysis of the Beaufort gyre freshwater content in 2003–2018. *J. Geophys. Res.: Oceans*, **124**, 9658–9689, https://doi.org/10.1029/2019JC015281.

Qiao, F. L., Y. L. Yuan, Y. Z. Yang, Q. A. Zheng, C. S. Xia, and J. Ma, 2004: Wave-induced mixing in the upper ocean: Distribution and application to a global ocean circulation model. *Geophys. Res. Lett.*, **31**, L11303, https://doi.org/10.1029/

2004GL019824.

Qiao, F. L., Z. Y. Song, Y. Bao, Y. J. Song, Q. Shu, C. J. Huang, and W. Zhao, 2013: Development and evaluation of an Earth System Model with surface gravity waves. *J. Geophys. Res.: Oceans*, **118**, 4514–4524, https://doi.org/10.1002/jgrc.20327.

Rabe, B., and Coauthors, 2014: Arctic Ocean basin liquid freshwater storage trend 1992–2012. *Geophys. Res. Lett.*, **41**, 961–968, https://doi.org/10.1002/2013GL058121.

Rantanen, M., A. Y. Karpechko, A. Lipponen, K. Nordling, O. Hyvärinen, K. Ruosteenoja, T. Vihma, and A. Laaksonen, 2022: The Arctic has warmed nearly four times faster than the globe since 1979. *Communications Earth & Environment*, **3**, 168, https://doi.org/10.1038/s43247-022-00498-3.

Redi, M. H., 1982: Oceanic Isopycnal mixing by coordinate rotation. *J. Phys. Oceanogr.*, **12**, 1154–1158, https://doi.org/10.1175/1520-0485(1982)012<1154:OIMBCR>2.0.CO;2.

Riahi, K., and Coauthors, 2017: The Shared Socioeconomic Pathways and their energy, land use, and greenhouse gas emissions implications: An overview. *Global Environmental Change*, **42**, 153–168, https://doi.org/10.1016/j.gloenvcha.2016.05.009.

Ricker, R., S. Hendricks, L. Kaleschke, X. Tian-Kunze, J. King, and C. Haas, 2017: A weekly Arctic sea-ice thickness data record from merged CryoSat-2 and SMOS satellite data. *The Cryosphere*, **11**, 1607–1623, https://doi.org/10.5194/tc-11-1607-2017.

Scholz, P., D. Sidorenko, S. Danilov, Q. Wang, N. Koldunov, D. Sein, and T. Jung, 2022: Assessment of the Finite-VolumE Sea ice–Ocean Model (FESOM2.0) – Part 2: Partial bottom cells, embedded sea ice and vertical mixing library CVMix. *Geoscientific Model Development*, **15**, 335–363, https://doi.org/10.5194/gmd-15-335-2022.

Serreze, M. C., and R. G. Barry, 2011: Processes and impacts of Arctic amplification: A research synthesis. *Global and Planetary Change*, **77**, 85–96, https://doi.org/10.1016/j.gloplacha.2011.03.004.

Shi, X. X., D. Notz, J. P. Liu, H. Yang, and G. Lohmann, 2021: Sensitivity of Northern Hemisphere climate to ice–ocean interface heat flux parameterizations. *Geoscientific Model Development*, **14**, 4891–4908, https://doi.org/10.5194/gmd-14-4891-2021.

Shu, Q., 2024a: Surface forcing (historical) for Arctic Ocean dynamical downscaling data establishment. Science Data Bank, https://doi.org/10.57760/sciencedb.16341.

Shu, Q., 2024b: Surface forcing (ssp245) for Arctic Ocean dynamical downscaling data establishment. Science Data Bank, https://doi.org/10.57760/sciencedb.16342.

Shu, Q., 2024c: Surface forcing (ssp585) for Arctic Ocean dynamical downscaling data establishment. Science Data Bank, https://doi.org/10.57760/sciencedb.16344.

Shu, Q., Q. Wang, Z. Y. Song, and F. L. Qiao, 2021: The poleward enhanced Arctic Ocean cooling machine in a warming climate. *Nature Communications*, **12**, 2966, https://doi.org/10.1038/s41467-021-23321-7.

Shu, Q., F. L. Qiao, Z. Y. Song, J. C. Zhao, and X. F. Li, 2018: Projected freshening of the Arctic Ocean in the 21st century. *J. Geophys. Res.: Oceans*, **123**, 9232–9244, https://doi.org/10.1029/2018JC014036.

Shu, Q., Q. Wang, J. Su, X. Li, and F. L. Qiao, 2019: Assessment of the Atlantic water layer in the Arctic Ocean in CMIP5 climate models. *Climate Dyn.*, **53**, 5279–5291, https://doi.org/10.1007/s00382-019-04870-6.

Shu, Q., Q. Wang, M. Årthun, S. Z. Wang, Z. Y. Song, M. Zhang, and F. L. Qiao, 2022: Arctic Ocean Amplification in a warming climate in CMIP6 models. *Science Advances*, **8**, eabn9755, https://doi.org/10.1126/sciadv.abn9755.

Shu, Q., F. L. Qiao, J. P. Liu, Y. Bao, and Z. Y. Song, 2024a: Description of FIO-ESM version 2.1 and evaluation of its sea ice simulations. *Ocean Modelling*, **187**, 102308, https://doi.org/10.1016/j.ocemod.2023.102308.

Shu, Q., and Coauthors, 2024b: Arctic Ocean dynamical downscaling data (ssp585) for understanding past and future climate change. Science Data Bank, https://doi.org/10.57760/sciencedb.16319.

Shu, Q., and Coauthors, 2024c: Arctic Ocean dynamical downscaling data (historical) for understanding past and future climate change. Science Data Bank, https://doi.org/10.57760/sciencedb.16206.

Shu, Q., and Coauthors, 2024d: Arctic Ocean dynamical downscaling data (ssp245) for understanding past and future climate change. Science Data Bank, https://doi.org/10.57760/sciencedb.16286.

Song, Z. Y., Y. Bao, D. Q. Zhang, Q. Shu, Y. J. Song, and F. L. Qiao, 2020: Centuries of monthly and 3-hourly global ocean wave data for past, present, and future climate research. *Scientific Data*, **7**, 226, https://doi.org/10.1038/s41597-020-0566-8.

Steele, M., R. Morley, and W. Ermold, 2001: PHC: A global ocean hydrography with a high-quality Arctic ocean. *J. Climate*, **14**, 2079–2087, https://doi.org/10.1175/1520-0442(2001)014<2079:PAGOHW>2.0.CO;2.

Stroeve, J., and D. Notz, 2018: Changing state of Arctic sea ice across all seasons. *Environmental Research Letters*, **13**, 103001, https://doi.org/10.1088/1748-9326/aade56.

Tebaldi, C., and Coauthors, 2021: Climate model projections from the Scenario Model Intercomparison Project (ScenarioMIP) of CMIP6. *Earth System Dynamics*, **12**, 253–293, https://doi.org/10.5194/esd-12-253-2021.

Tsujino, H., and Coauthors, 2018: JRA-55 based surface dataset for driving ocean–sea-ice models (JRA55-do). *Ocean Modelling*, **130**, 79–139, https://doi.org/10.1016/j.ocemod.2018.07.002.

Wang, Q., and S. Danilov, 2022: A synthesis of the upper Arctic Ocean circulation during 2000–2019: Understanding the roles of wind forcing and sea ice decline. *Frontiers in Marine Science*, **9**, 863204, https://doi.org/10.3389/fmars.2022.863204.

Wang, Q., C. Wekerle, S. Danilov, X. Z. Wang, and T. Jung, 2018: A 4.5 km resolution Arctic Ocean simulation with the global multi-resolution model FESOM 1.4. *Geoscientific Model Development*, **11**, 1229–1255, https://doi.org/10.5194/gmd-11-1229-2018.

Wang, Q., S. Danilov, D. Sidorenko, R. Timmermann, C. Wekerle, X. Wang, T. Jung, and J. Schröter, 2014: The Finite Element Sea Ice-Ocean Model (FESOM) v. 1.4: Formulation of an ocean general circulation model. *Geoscientific Model Development*, **7**, 663–693, https://doi.org/10.5194/gmd-7-663-2014.

Wang, Q., C. Wekerle, S. Danilov, D. Sidorenko, N. Koldunov, D. Sein, B. Rabe, and T. Jung, 2019: Recent sea ice decline did not significantly increase the total liquid freshwater content of the Arctic Ocean. *J. Climate*, **32**, 15–32, https://doi.org/10.1175/JCLI-D-18-0237.1.

Wang, Q., and Coauthors, 2020: Intensification of the Atlantic water supply to the Arctic Ocean through Fram strait induced by Arctic sea ice decline. *Geophys. Res. Lett.*, **47**, e2019GL086682, https://doi.org/10.1029/2019GL086682.

Wang, Q., and Coauthors, 2023: A Review of Arctic–Subarctic ocean linkages: Past changes, mechanisms, and future projections. *Ocean-Land-Atmosphere Research*, **2**, 0013, https://doi.org/10.34133/olar.0013.

Wang, Q., and Coauthors, 2024: Impact of increased resolution on Arctic Ocean simulations in Ocean Model Intercomparison Project phase 2 (OMIP-2). *Geoscientific Model Development*, **17**, 347–379, https://doi.org/10.5194/gmd-17-347-2024.

Wang, S. Z., Q. Wang, M. Y. Wang, G. Lohmann, and F. L. Qiao, 2022: Arctic Ocean freshwater in CMIP6 coupled models. *Earth's Future*, **10**, e2022EF002878, https://doi.org/10.1029/2022EF002878.

Yang, X. D., Y. Bao, Z. Y. Song, Q. Shu, Y. J. Song, X. Wang, and F. L. Qiao, 2023: Key to ENSO phase-locking simulation: Effects of sea surface temperature diurnal amplitude. *npj Climate and Atmospheric Science*, **6**, 159, https://doi.org/10.1038/s41612-023-00483-3.

Yu, L., J. P. Liu, Y. Q. Gao, and Q. Shu, 2022: A sensitivity study of Arctic ice-ocean heat exchange to the three-equation boundary condition parametrization in CICE6. *Adv. Atmos. Sci.*, **39**, 1398–1416, https://doi.org/10.1007/s00376-022-1316-y.

Zanowski, H., A. Jahn, and M. M. Holland, 2021: Arctic Ocean freshwater in CMIP6 ensembles: Declining sea ice, increasing ocean storage and export. *J. Geophys. Res.: Oceans*, **126**, e2020JC016930, https://doi.org/10.1029/2020JC016930.

Zhang, M. Z., Z. F. Xu, Y. Han, and W. D. Guo, 2024: Evaluation of CMIP6 models toward dynamical downscaling over 14 CORDEX domains. *Climate Dyn.*, **62**, 4475–4489, https://doi.org/10.1007/s00382-022-06355-5.